Nanoscale

PAPER

View Article Online
View Journal | View Issue





Cite this: *Nanoscale*, 2018, **10**, 8642

# Facet-selective deposition of Au and Pt on Ag nanocubes for the fabrication of bifunctional Ag@Au–Pt nanocubes and trimetallic nanoboxes†

Zhiwei Zhang,[a,b] Jaewan Ahn,[a] Junki Kim,[a] Zhengyun Wu[b] and Dong Qin *[a]

Received 2nd March 2018,
Accepted 9th April 2018

DOI: 10.1039/c8nr01794h

rsc.li/nanoscale

We report a facile route to the synthesis of Ag@Au–Pt trimetallic nanocubes in which the Ag, Au, and Pt atoms are exposed at the corners, side faces, and edges, respectively. Our success relies on the use of Ag@Au nanocubes, with $Ag_2O$ patches at the corners and Au on the side faces and edges, as seeds for the site-selective deposition of Pt on the edges only in a reaction system containing ascorbic acid ($H_2Asc$) and poly(vinylpyrrolidone). At an initial pH of 3.2, $H_2Asc$ can dissolve the $Ag_2O$ patches, exposing the Ag atoms at the corners of a nanocube. Upon the injection of the $H_2PtCl_6$ precursor, the Pt atoms derived from the reduction by both $H_2Asc$ and Ag are preferentially deposited on the edges, leading to the formation of Ag@Au–Pt trimetallic nanocubes. We demonstrate the use of 2,6-dimethylphenyl isocyanide as a molecular probe to confirm and monitor the deposition of Pt atoms on the edges of nanocubes through surface-enhanced Raman scattering (SERS). We further explore the use of these bifunctional trimetallic nanoparticles with integrated plasmonic and catalytic properties for *in situ* SERS monitoring the reduction of 4-nitrothiophenol by $NaBH_4$. Upon the removal of Ag *via* $H_2O_2$ etching, the Ag@Au–Pt nanocubes evolve into trimetallic nanoboxes with a wall thickness of about 2 nm and well-defined openings at the corners. The trimetallic nanoboxes embrace plasmon resonance peaks in the near-infrared region with potential in biomedical applications.

## Introduction

Multimetallic nanocrystals are exciting for a number of applications that include catalysis,[1–10] plasmonics[11–14] and surface-enhanced Raman scattering (SERS).[15–18] The excitement mainly arises from the synergetic effects between different metals, which can greatly enhance the properties relative to their monometallic counterparts. For example, we have demonstrated that the deposition of a second metal such as Pt or Pd on the surface of Ag nanocrystals can integrate both plasmonic and catalytic properties in individual nanocrystals.[14–16] Many other groups have also reported the greatly enhanced reactivity/selectivity of bimetallic nanocrystals in catalysis because of the synergetic effects between different metals.[1] Among the various parameters, including composition, size, shape, and structure (solid *versus* hollow), the shape of nanocrystals plays an essential role in controlling the properties for specific applications. It is well-established that the shape of Ag or Au nanocrystals not only controls their localized surface plasmon resonance (LSPR) properties but also their performance in applications such as SERS.[11,14] On the other hand, it has become an active subject of research in recent years to enhance the activity and/or selectivity of nanocatalysts by engineering the shape of nanocrystals to ensure that the most active and/or selective facet will be presented on the surface in the greatest proportion.[19] In addition to these benefits, the presence of a well-defined, single type of facet on the surface of a catalyst will make it much easier to elucidate the reaction mechanism.[20] Taken together, there is a strong need to develop methods capable of generating multimetallic nanocrystals with well-defined and controllable shapes.

Compared with the great success for both monometallic and bimetallic systems,[12,21] there are very few reports on the preparation of trimetallic nanocrystals with well-defined shapes and morphologies. Three strategies are documented in the literature. The first one relies on the use of one-pot synthesis to generate core–shell trimetallic nanoparticles. To this end, Yamauchi and co-workers synthesized and characterized Au@Pd–Pt core–shell nanoparticles consisting of the Au core, the Pd inner layer and the dendritic Pt outer shell.[22,23] Han and co-workers reported the synthesis of Au@Pd–Pt core–shell

[a]*School of Materials Science and Engineering, Georgia Institute of Technology, Atlanta, Georgia 30332, USA. E-mail: dong.qin@mse.gatech.edu*
[b]*Department of Physics, Xiamen University, Xiamen 361005, Fujian Province, P. R. China*

†Electronic supplementary information (ESI) available. See DOI: 10.1039/c8nr01794h

nanocrystals with a well-defined Au octahedral core and Pd–Pt alloy shell.[24] The second strategy involves the use of seed-mediated co-reduction. To this end, Skrabalak and co-workers demonstrated the synthesis of Au@Pd–Ag octopods with well-defined shapes or morphologies.[25] The third strategy relies on the use of the galvanic replacement reaction and the Kirkendall effect to generate Ag–Au–Pd hollow nanostructures.[26] Despite these reports, it remains elusive to fabricate trimetallic nanocrystals with the distinctive elements being exposed on different types of facets.

Herein, we report a facile approach to the synthesis of Ag@Au–Pt trimetallic nanocubes with the Au and Pt atoms being selectively exposed on the side faces and edges, respectively, of Ag nanocubes. First, we use our published protocol to produce Ag@Au nanocubes with $Ag_2O$ patches at the corners and conformal Au overlayers on the side faces and edges.[27,28] We then disperse the as-obtained nanocrystals in an aqueous solution containing ascorbic acid ($H_2Asc$) and poly(vinylpyrrolidone) (PVP) at pH = 3.2. Under an acidic conditions, the $Ag_2O$ patches at the corners of nanocubes will be etched away by the $H_2Asc$,[29,30] exposing the Ag atoms underneath. When the $H_2PtCl_6$ precursor is injected into the reaction solution, the Pt atoms derived from the reduction by Ag (*via* galvanic replacement) and $H_2Asc$ will be preferentially deposited on the edges, or {110} facets, of the Ag@Au nanocubes, leading to the formation of Ag@Au–Pt nanocubes with the three elements exposed on different facets. We further demonstrate that the Ag@Au–Pt nanocubes embrace a strong SERS activity when used with an SERS probe such as 2,6-dimethylphenyl isocyanide (2,6-DMPI). Remarkably, this molecular probe can be used to report the deposition of Pt atoms on the edges of the Ag@Au nanocubes with a sensitivity approaching a monolayer. We also explore the bifunctional Ag@Au–Pt nanocubes with combined plasmonic and catalytic properties as an SERS probe for the *in situ* monitoring of the reduction of 4-nitrothiophenol (4-NTP) by $NaBH_4$. We identify that the reduction rate can be significantly accelerated when Ag@Au–Pt nanocubes are introduced as catalysts in comparison with the case of Ag@Au nanocubes. When the Ag cores are removed with aqueous $H_2O_2$, the Ag@Au–Pt nanocubes are transformed into Ag–Au–Pt nanoboxes with a wall thickness of about 2 nm, together with well-defined openings at the corner sites. The trimetallic nanoboxes embrace strong plasmon resonance, with a major LSPR peak in the near infrared region.

# Experimental

### Chemicals and materials

Silver trifluoroacetate ($CF_3COOAg$, 98%), poly(vinylpyrrolidone) with an average molecular weight of 55 000 (PVP-55), sodium hydrosulfide hydrate ($NaHS{\cdot}xH_2O$), aqueous hydrochloric acid (HCl, 37%), L-ascorbic acid ($H_2Asc$, 99%), sodium hydroxide (NaOH, 98+%), gold(III) chloride trihydrate ($HAuCl_4{\cdot}3H_2O$, 99.9+%), chloroplatinic acid hexahydrate ($H_2PtCl_6{\cdot}6H_2O$, 37.5%), hydrogen peroxide ($H_2O_2$, 30 wt% in $H_2O$), 2,6-dimethylphenylisocyanide (2,6-DMPI, ≥98.0%), acetone (99.5+%), sodium borohydride ($NaBH_4$, 99.99%) and 4-nitrothiophenol (4-NTP, 80%) were all purchased from Sigma-Aldrich. Ethylene glycol (EG) was purchased from J. T. Baker. All chemicals were used as received. All aqueous solutions were prepared using deionized (DI) water with a resistivity of 18.2 MΩ cm at room temperature.

### Synthesis of Ag nanocubes

We followed the reported protocol to synthesize Ag nanocubes with an average edge length of 37.5 ± 1.5 nm.[31] The nanocubes were washed with acetone and DI water three times before they were redispersed in DI water for future use.

### Synthesis of Ag@Au core–shell nanocubes

In a typical synthesis, 2 mL of PVP-55 solution (1 mM) was introduced into a 23 mL glass vial, followed by the addition of 0.5 mL of $H_2Asc$ (0.1 M), 0.5 mL of aqueous NaOH solution (0.2 M) and 0.02 mL of the aqueous suspension of Ag nanocubes (with a final concentration of $6.8 \times 10^{10}$ particles per mL) under magnetic stirring. Next, 0.8 mL of aqueous $HAuCl_4$ solution (0.1 mM) was titrated into the mixture using a syringe pump at a rate of 0.02 mL $min^{-1}$. After the completion of titration, the product was collected by centrifugation at 6000 rpm for 15 min and dispersed in 0.05 mL DI water for further use.

### Synthesis of Ag@Au–Pt trimetallic nanocubes

In a typical synthesis, 2 mL of PVP-55 solution (1 mM) was introduced into a 23 mL glass vial, followed by the addition of 0.5 mL of $H_2Asc$ (0.1 M) and 0.05 mL of the as-prepared Ag@Au nanocubes (with a final concentration of $7.6 \times 10^{10}$ particles per mL) under magnetic stirring for 10 min. Next, different volumes of aqueous $H_2PtCl_6$ solution (0.2 mM) was injected into the mixture using a pipette (10 μL for every shot at an interval of 30 s). The reaction solution was maintained under magnetic stirring at room temperature for another 10 min once the injection had been completed. The product was collected by centrifugation at 4600 rpm for 20 min and dispersed in DI water for further use.

### Preparation of Ag–Au nanoboxes and Ag–Au–Pt nanoboxes

We mixed 0.1 mL of the as-prepared Ag@Au nanocubes with 0.6 mL of PVP-55 (1 mM) and 0.4 mL of $H_2Asc$ (0.1 M), and incubated them for 20 min before we collected the particles by centrifugation at 5000 rpm for 15 min. These treated Ag@Au nanocubes (0.1 mL with a concentration of $7.6 \times 10^{11}$ particles per mL) were then mixed with 1 mL of 3% aqueous $H_2O_2$ and incubated at room temperature for 2 h. The same etching protocol was also applied to Ag@Au–Pt nanocubes (0.1 mL, with a concentration of $7.6 \times 10^{11}$ particles per mL) for the fabrication of Ag–Au–Pt nanoboxes. The resultant products were washed twice with water and re-dispersed in 0.5 mL of water.

### Instrumentation and characterization

The UV-vis spectra were recorded using a Cary 50 spectrometer (Agilent Technologies, Santa Clara, CA). The quantitative

measurement of Pt, Au and Ag contents was performed using an inductively coupled plasma mass spectrometer (ICP-MS, NexION 300Q, PerkinElmer, Waltham, MA). A routine centrifuge (Eppendorf 5430) was used for the collection and washing of samples and the preparation of the ICP-MS samples. Transmission electron microscopy (TEM) images were taken using a Hitachi HT7700 microscope (Hitachi, Tokyo, Japan) operating at 120 kV. Raman spectra were taken using a Renishaw InVia micro Raman system (Renishaw, Hoffman Estates, IL). High-resolution TEM images were taken using an F30 FEI TEM and a Hitachi HD2700 $C_s$-corrected microscope operated at 200 kV. The energy-dispersive X-ray spectroscopy (EDS) images were acquired from an EDS detector on the HD2700 microscope. The XPS spectra were collected using a Thermo K-Alpha X ray photoelectron spectrometer (Thermo Fisher Scientific, Waltham, MA).

### XPS analysis of Ag@Au–Pt nanocubes

Approximately 20 μL of the as-prepared sample suspension was dropcasted on the surface of a 1 × 1 $cm^2$ silicon wafer and allowed to dry overnight under ambient conditions in air. The sample was then loaded into a Thermo K-Alpha X ray photoelectron spectrometer and the Au 4f (79–95 eV), Ag 3d (360–380 eV) and Pt 4f (65–80 eV) regions of the sample were measured with a 0.1 eV resolution.

### Conversion of original EDS mapping results to line-scan data

The raw data from the EDS mapping of each element was first converted into greyscale, and the region of interest was defined to be 600 pixels long and 80 pixels tall. The linescan plot was generated by plotting the sum of all intensity values within each column of pixels (*y*-axis) for all 600 columns of pixels (*x*-axis). The raw scale bar was used to calibrate the real values for the distance of each position on the *x*-axis. Each data point was connected to the next with a straight line.

### SERS measurements

The as-prepared Ag@Au and Ag@Au–Pt nanocubes were functionalized with a $10^{-5}$ M ethanol solution of 2,6-DMPI for 2 h. After washing with water twice, the 2,6-DMPI-functionalized nanoparticles were redispersed in water to attain a concentration of approximately 5.5 × $10^{10}$ particles per mL. The Raman spectra were taken using a Renishaw inVia Raman spectrometer coupled with a Leica microscope using a 100× objective. The excitation wavelength was 532 nm, in conjunction with a grating of 2400 lines per mm, at a power of 10% of the laser output (50 mW). Data were collected from the solution phase with a collection time of 10 s for all samples. A sample cell was fabricated from a polydimethylsiloxane (PDMS) block by punching a small hole to hold 20 μL of liquid sample. After the PDMS was attached to a glass slide, we loaded the sample solution and then placed a glass coverslip of 170 μm thickness on top of the PDMS to prevent solvent evaporation.

### *In situ* SERS monitoring of the reduction of 4-NTP by Ag@Au nanocubes and Ag@Au–Pt nanocubes

The Ag@Au and Ag@Au@Pt nanocubes were dispersed in ethanol solution 4-NTP ($10^{-6}$ M) and incubated at room temperature for 1 h. The 4-NTP-functionalized particles were then washed with DI water twice and redispersed in DI water to achieve a concentration of approximately 1.4 × $10^{11}$ particles per mL. Upon mixing 200 μL of the suspension with 60 or 200 μL of aqueous $NaBH_4$ (0.1 mg $mL^{-1}$) in a 1.5 mL centrifuge tube, the products were allowed to catalyze the 4-NTP reduction reaction at room temperature. We then withdrew 20 μL of sample from the reaction solution every several minutes and placed this sample in a PDMS-based cell for collecting the SERS spectra using a 5× objective, together with a data collection time of 7 s at a power of 100% of the output of a 532 nm laser (50 mW).

## Results and discussion

We first prepared Ag nanocubes with an average edge length of 37.5 ± 1.5 nm by following the published protocol (Fig. S1†).[31] Fig. 1 shows a schematic illustration of how to transform Ag nanocubes into Ag@Au–Pt trimetallic nanocubes. In the first step, we titrate aqueous $HAuCl_4$ into an aqueous suspension of Ag nanocubes in the presence of $H_2Asc$ (a reducing agent), PVP (a stabilizer), and NaOH (a pH modifier) at an initial pH of 11.8 using a syringe pump. Based on our published study,[30] we argue that the added $HAuCl_4$ should first react with the Ag

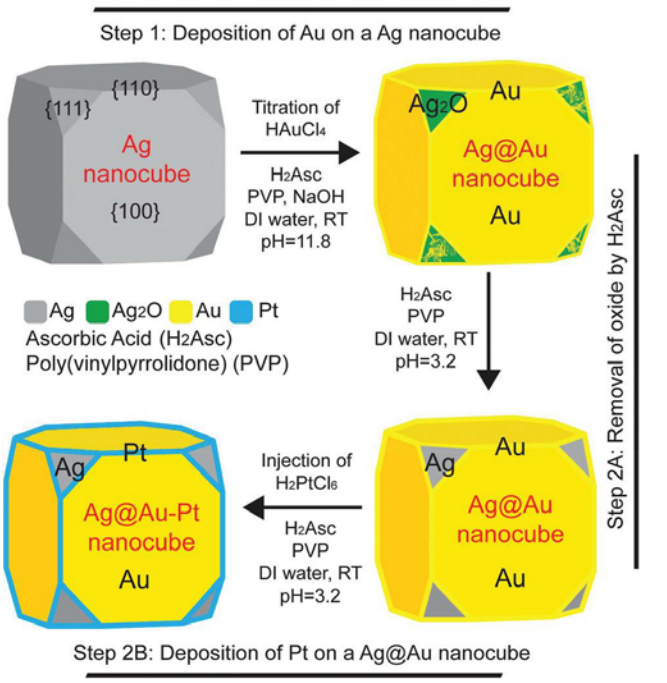


**Fig. 1** Schematic illustration of a proposed pathway responsible for the transformation of an Ag nanocube into an Ag@Au core–shell nanocube and then an Ag@Au–Pt nanocube.

atoms positioned on the {111} facets (*i.e.*, corners) of the nanocube for the deposition of Au atoms on the {110} facets (*i.e.*, edges) through a galvanic replacement mechanism. The released $Ag^+$ ions should react immediately with the $OH^-$ ions for the formation of $Ag_2O$ patches at the corners, terminating the galvanic replacement reaction. Meanwhile, the added $HAuCl_4$ undergoes ligand exchange with $OH^-$ to form $AuCl(OH)_3^-$ and $Au(OH)_4^-$ before they are reduced by the ascorbate monoanion ($HAsc^-$) to generate Au atoms for their deposition onto the entire surface of each nanocube. Combined together, Ag nanocubes are transformed into Ag@Au core–shell nanocubes, together with $Ag_2O$ patches under the Au overlayers at the corner sites. In the second step, we disperse the as-obtained Ag@Au nanocubes in an aqueous solution containing $H_2Asc$ and PVP under magnetic stirring for 10 min. At an initial pH of 3.2, $H_2Asc$ can dissolve the $Ag_2O$ patches, exposing the underlying Ag atoms at the corners. Upon the injection of aqueous $H_2PtCl_6$, the Pt atoms derived from the reduction of $H_2PtCl_6$ by both Ag and $H_2Asc$ are selectively deposited on the edges, leading to the formation of Ag@Au–Pt trimetallic nanocubes with the Ag, Au and Pt atoms spatially confined to the {111}, {100} and {110} facets, respectively.

Fig. 2A shows a transmission electron microscopy (TEM) image of the as-obtained Ag@Au nanocubes obtained after titrating 0.8 mL of aqueous $HAuCl_4$ (see the Experimental section for details). The cubic shape was largely preserved in the products, while the average edge length was increased from 37.5 ± 1.5 nm to 39.9 ± 1.7 nm. After treating the sample with $H_2Asc$ for 20 min and then incubating with aqueous $H_2O_2$ for 2 h, Fig. 2B shows the formation of nanoboxes with well-defined openings at the corners, consistent with our previous findings.[30] Fig. 2C shows the TEM image of the Ag@Au–Pt nanocubes corresponding to the injection of 10 μL of aqueous $H_2PtCl_6$. Again, there was very little change in the morphology but the average edge length was further increased to 40.4 ± 1.6 nm. After etching with aqueous $H_2O_2$, Fig. 2D shows a TEM image of the resultant structures, indicating the formation of nanoboxes with a cubic shape and well-defined pores at the corners. When the injection volume of $H_2PtCl_6$ was increased to 50 μL, Fig. 2E shows a typical TEM image of the products. We noticed that the particles still took a cubic shape, with slightly sharpened corners under projection. The edge length was increased to 41.6 ± 1.3 nm, suggesting that more Pt atoms were deposited on the edges. After treatment with aqueous $H_2O_2$, Fig. 2F shows the formation of cubic nanoboxes similar to those shown in Fig. 2D except that the edges became rougher, likely because of the deposition of more Pt atoms. To confirm the deposition of Pt on the Ag@Au nanocubes, we used ICP-MS to measure the Pt content. It was found that the amount of Pt was increased from 0.05 to 0.20 wt% as the injection volume of $H_2PtCl_6$ solution was increased from 10 to 50 μL. Fig. S2† compares the X-ray photoelectron spectroscopy (XPS) data of these two samples. We observed an increase in the amount of Pt deposited on the Ag@Au nanocubes as the injection volume was increased, consistent with the ICP-MS results.

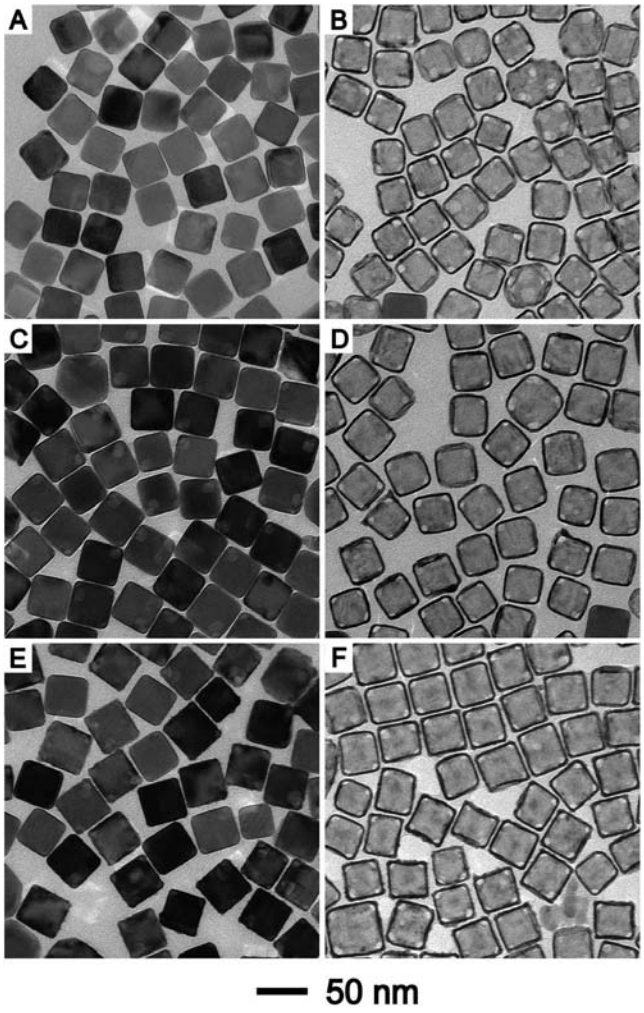


**Fig. 2** TEM images of (A) Ag@Au nanocubes and (C, E) Ag@Au nanocubes after reaction with (C) 10 μL and (E) 50 μL volumes of 0.2 mM aqueous $H_2PtCl_6$. (B, D, F) TEM images of the products after etching the samples in (A, C, E) with 3% aqueous $H_2O_2$.

We also used energy dispersive X-ray spectroscopy (EDS) mapping to examine the distributions of constituent elements on an individual trimetallic nanocube. Fig. 3A shows an aberration-corrected high-angle annular dark-field scanning TEM (HAADF-STEM) image taken from a trimetallic nanocube prepared with the addition of 0.8 mL of aqueous $HAuCl_4$ and 50 μL of aqueous $H_2PtCl_6$. When the nanocube was oriented along the ⟨001⟩ zone axis, Fig. 3B–D shows the spatial distributions of Ag, Au, and Pt. We noticed that the distribution of Ag was confined to a solid square while Au was largely deposited around the nanocube. Under the experimental conditions, it is anticipated that the amount of Au being deposited on the surface of each Ag nanocube was adequate to form a complete shell six atomic layers thick.[27] As such, it is difficult to resolve the difference in thickness between the Au overlayers deposited on {111} and {100} facets. On the other hand, the Pt signals appeared to be slightly stronger on the edges compared with those on the side faces and corners.

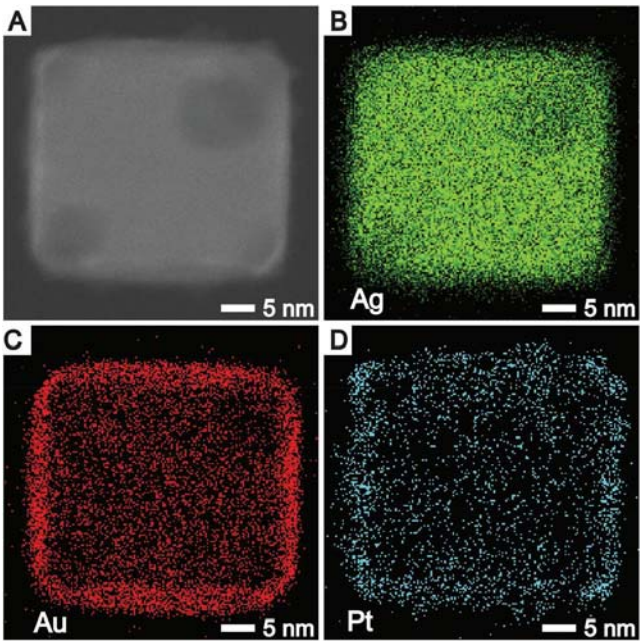


Fig. 3 (A) HAADF-STEM image recorded from one of the Ag@Au–Pt nanocubes prepared with the introduction of 50 μL of aqueous $H_2PtCl_6$ (Fig. 2E), with the particle being orientated along the ⟨001⟩ zone axis. (B–D) EDS mapping of the same nanocube (green: Ag; red: Au; blue: Pt).

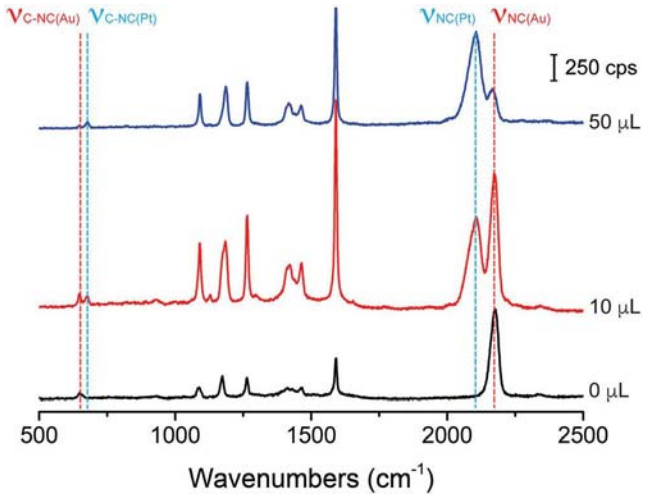


Fig. 4 SERS spectra recorded from aqueous suspensions of 2,6-DMPI-functionalized samples prepared by reacting the Ag@Au nanocubes with different volumes of aqueous $H_2PtCl_6$.

Based on the EDS mapping results of the Ag@Au–Pt nanocube shown in Fig. S3A,† we performed an analysis to construct the line-scan data by defining a region of interest (see more details in the Experimental section). Fig. S3B† shows the result of our analysis, supporting our argument that more Pt atoms would be deposited on the edges of nanocubes. Fig. S3A and B† also suggest that we could identify some Ag atoms on the outermost surface of an Ag@Au nanocube. During the deposition of Pt on the Ag@Au nanocubes in the presence of $H_2Asc$, we argue that some $H_2PtCl_6$ could react with Ag atoms of the Ag@Au nanocubes *via* the galvanic replacement reaction, leading to the formation of $Ag^+$ ions in the reaction solution. Likely, these released $Ag^+$ ions and the $H_2PtCl_6$ could be co-reduced by $H_2Asc$ to generate Ag atoms and Pt atoms followed by their co-deposition on Ag@Au nanocubes.

To verify the formation of Ag@Au–Pt nanocubes, we used 2,6-dimethylphenyl isocyanide (2,6-DMPI) as a molecular probe to detect the deposition of Pt on the edges of the Ag@Au nanocubes by surface-enhanced Raman scattering (SERS). In a recent study, we demonstrated the use of 2,6-DMPI for monitoring *in situ* the deposition of Pt on Ag nanocubes.[32] Because the sites for preferential heterogeneous nucleation and the SERS hot spots coincide at the edges of a Ag nanocube, this new detection paradigm allows for unprecedented sensitivity, with a lower detection limit below one monolayer. More interestingly, the stretching frequency for the NC bond would be different when the isocyanide group binds to the Ag and Pt atoms, respectively, making it feasible to characterize the Pt atoms located on the edges of the Ag nanocube by following the $\nu_{NC}$ stretching frequency and the peak intensity. Fig. 4 shows the SERS spectra of 2,6-DMPI adsorbed onto the Ag@Au nanocubes before and after they had reacted with different volumes of $H_2PtCl_6$, with an excitation wavelength at 532 nm. Before the injection of $H_2PtCl_6$, the spectrum showed two characteristic peaks at 2177 and 648 $cm^{-1}$, which could be assigned to the NC stretching, $\nu_{NC(Au)}$, and C-NC stretching, $\nu_{C-NC(Au)}$, bands, respectively, of 2,6-DMPI adsorbed onto Au.[33] The remaining peaks were associated with the ring-associated bands of 2,6-DMPI.[34] At an injection volume of 10 μL, in addition to the major $\nu_{NC(Au)}$ and $\nu_{C-NC(Au)}$ peaks, we resolved two new peaks at 2105 and 675 $cm^{-1}$, which could be assigned to the $\nu_{NC(Pt)}$ and $\nu_{C-NC(Pt)}$ bands, respectively, of 2,6-DMPI adsorbed onto Pt. At 50 μL, the $\nu_{NC(Pt)}$ and $\nu_{C-NC(Pt)}$ bands became predominant with a decrease in peak intensity for both $\nu_{NC(Au)}$ and $\nu_{C-NC(Au)}$ bands, indicating more Pt atoms being deposited on the edges of the nanocubes. Taken together, this set of SERS data provided a strong evidence to support the deposition of Pt on the edges of Ag@Au nanocubes.

To further confirm the deposition of Pt, we used $H_2O_2$ etching to remove Ag from the sample obtained with 50 μL of $H_2PtCl_6$ solution. Fig. 5A shows the aberration-corrected high-angle annular bright-field scanning TEM (HAABF-STEM) image of one such nanobox shown in Fig. 2F. Fig. 5B shows the atomic-resolution HAABF-STEM image recorded from the corner region of a nanobox. We could resolve the highly ordered arrangement for the atoms on the side faces, confirming the deposition of Au on the {100} facets of the nanocube. However, it was difficult to distinguish individual atoms on the edges because of the deposition of Pt to generate an Ag–Au–Pt alloy. The wall thickness of the nanobox was about 2 nm. On the other hand, as indicated by the white, dashed lines, we observed a well-defined opening at the corner from the STEM image, suggesting that exposed Ag atoms were located on the {111} facets and they could be removed during

 

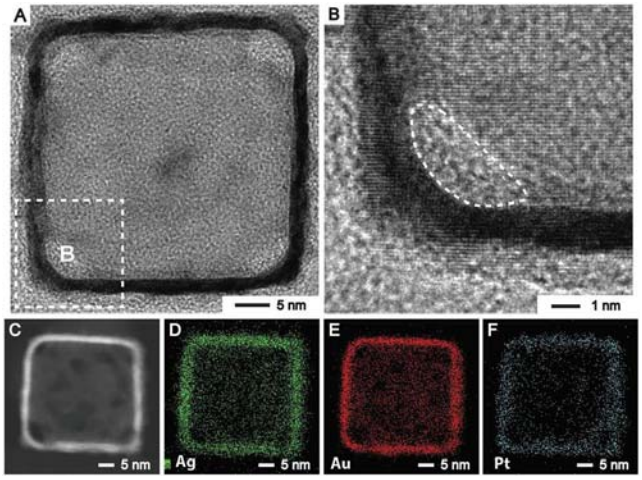


Fig. 5 (A) HAABF-STEM image taken from one of the Ag@Au–Pt nanoboxes shown in Fig. 2F, with the particle orientated at the ⟨001⟩ zone axis. (B) Atomic-resolution HAABF-STEM image taken from the corner region of a nanobox (marked by the white dashed box). (C–F) STEM image and EDS mapping of Ag (green), Au (red), and Pt (blue) for an individual nanobox shown in (C).

$H_2O_2$ etching. Fig. 5C shows the STEM image of another nanobox in Fig. 2F when it was oriented along the ⟨001⟩ zone axis. Fig. 5D–F show the spatial distributions of Ag, Au, and Pt for the same nanobox, respectively, together with openings at the corners. By using the EDS mapping data of the Ag–Au–Pt nanobox shown in Fig. S3C,† we conducted the above-mentioned analysis to obtain line-scan data across a region of interest. Fig. S3D† shows that Ag, Au, and Pt were mainly confined to the edges. It is also worth mentioning that the EDS results show that the size of Au is slightly smaller than that of Ag, suggesting the presence of Ag on the surface of Au. This observation would further support our argument of the presence of Ag on the surface of Ag@Au nanocubes (see Fig. S3A and B†). Our ICP-MS analysis indicated that the nanoboxes had an elemental composition of $Ag_{57}Au_{41}Pt_2$, consistent with our EDS data.

The Ag@Au–Pt nanocubes could serve as an *in situ* SERS probe for monitoring the reduction of 4-nitrothiophenol (4-NTP) to 4-aminothiophenol (4-ATP). In a typical process, we functionalized the as-prepared nanoparticles with 4-NTP and collected SERS spectra at different time points. Fig. 6A shows the SERS spectra captured during the reaction as it was catalyzed by Au@Au nanocubes. At $t$ = 0, we identified three characteristic bands of 4-NTP located at 1110, 1338, and 1572 $cm^{-1}$ (labeled by red dashed lines), corresponding to C–N stretching ($\nu_{CN}$), O–N–O stretching ($\nu_{NO_2}$), and C–C stretching ($\nu_{CC}$), respectively. The peak located at 1080 $cm^{-1}$ could be assigned to C–S stretching ($\nu_{CS}$). At $t$ = 10 min, the $\nu_{NO_2}$ of 4-NTP was red-shifted from 1338 to 1333 $cm^{-1}$, together with a decrease in its intensity. Also, the intensities of $\nu_{CN}$ and $\nu_{CC}$ bands were decreased while the peak positions remained essentially the same. At this time point, a new band emerged at 1595 $cm^{-1}$, which can be assigned to $\nu_{CC}$ of 4-ATP (marked

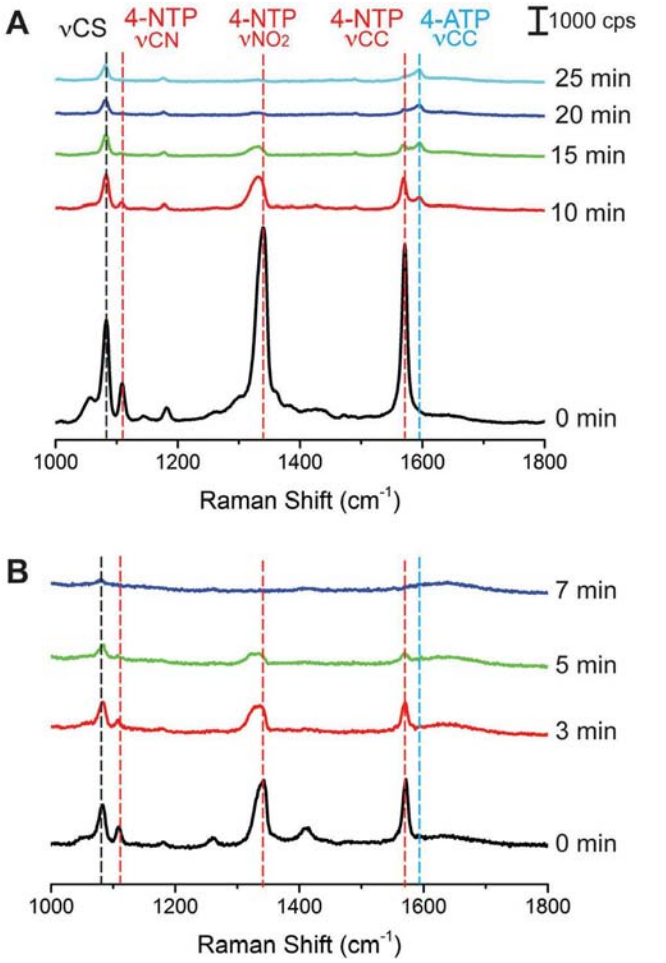


Fig. 6 SERS spectra recorded during the reduction of 4-NTP to 4-ATP by 200 μL of 0.1 mg $mL^{-1}$ $NaBH_4$ using (A) Ag@Au and (B) Ag@Au–Pt nanocubes, respectively, as the catalysts.

by a blue dashed line). As the reaction progressed to 15 min and then to 20 min, we noticed that the $\nu_{NO_2}$ of 4-NTP started to decrease in intensity, together with a slight shift to the blue. During this period, the $\nu_{CC}$ of 4-NTP continuously decreased in intensity as that of 4-ATP gradually increased in intensity. At $t$ = 25 min, all three bands associated with the 4-NTP disappeared while the $\nu_{CC}$ band of 4-ATP remained, indicating the completion of the reaction. It is worth noting that the peak of $\nu_{CS}$ at 1083 $cm^{-1}$ was relatively stable during the course of the reaction, suggesting the molecules likely remained on the surface because of thiolate bonding. It is also worth mentioning that the intensity of the band at 1595 $cm^{-1}$ for 4-ATP was 15 times weaker than the band at 1572 $cm^{-1}$ for 4-NTP. This result suggests the desorption of 4-ATP from the surface of the nanocubes because of a strong binding of $BH_4^-$ to the surface of the nanocubes.[35]

Fig. 6B shows the time-elapsed SERS spectra using the Ag@Au–Pt nanocubes (obtained with 10 μL of $H_2PtCl_6$ solution) as the catalyst while keeping all other experimental parameters the same. At $t$ = 0 min, we observed a 65% decrease in intensity for the 4-NTP peak at 1572 $cm^{-1}$ ($\nu_{CC}$) relative to the

case of the Ag@Au nanocubes. We suspected that the deposition of Pt atoms on the edges of Ag–Au nanocubes could deteriorate the SERS activity of Au.[32] Such a decrease could also arise from the less efficient adsorption of 4-NTP molecules on the Pt surface. When the reaction progressed to 3 and then to 5 min after the addition of $NaBH_4$, we observed the gradual decrease in peak intensity for all three 4-NTP bands, indicating the reduction of 4-NTP to 4-ATP. However, it was difficult to resolve the $\nu_{CC}$ band of 4-ATP at 1595 $cm^{-1}$ because of the desorption of 4-ATP from the surface in the presence of $BH_4^-$, consistent with the results shown in Fig. 6A. At $t$ = 7 min, the spectrum only showed one small peak at 1083 $cm^{-1}$ ($\nu_{CS}$), indicating the completion of the reaction. Taken together, we argue that the introduction of a small amount of Pt to the surface of the Ag@Au nanocubes would significantly accelerate the reduction of 4-NTP by $NaBH_4$. In order to confirm the production of 4-ATP, we performed another control experiment by adding 60 μL of $NaBH_4$ solution (0.1 mg $mL^{-1}$) to initiate the reaction. Fig. S4† shows the SERS spectra collected at 20 min by benchmarking against those in the absence of $NaBH_4$ and the presence of $NaBH_4$ at 200 μL, respectively. When we decreased the amount of $NaBH_4$ involved to reduce the reaction rate, we were able to observe the $\nu_{CC}$ band of 4-ATP at 1595 $cm^{-1}$, confirming the reduction of 4-NTP to 4-ATP by $NaBH_4$ on the surface of the Ag@Au–Pt nanocubes. Taken together, we believe that the Ag@Au–Pt nanocubes are better catalysts for the reduction of 4-NTP by $NaBH_4$ compared with the Ag@Au nanocubes.

We also used UV-vis-NIR spectroscopy to characterize the optical properties of the as-obtained Ag@Au–Pt nanocubes and the resultant nanoboxes after etching with aqueous $H_2O_2$. Fig. 7A shows that the major LSPR peak of the Ag nanocubes was red-shifted from 428 to 438 nm for the Ag@Au nanocubes upon the reaction with 0.8 mL of $HAuCl_4$ solution, followed by another slight red-shift to 444 nm after the reaction of the Ag@Au nanocubes with 50 μL $H_2PtCl_6$ solution. These results suggest that the LSPR properties of the Ag nanocubes were largely preserved in both the Ag@Au and Ag@Au–Pt nanocubes. When the solid nanoparticles were transformed into nanoboxes through the removal of Ag, Fig. 7B indicates that the LSPR peaks of the resultant Ag–Au and Ag–Au–Pt nanoboxes were significantly red-shifted to 1070 and to 1090 nm, respectively.

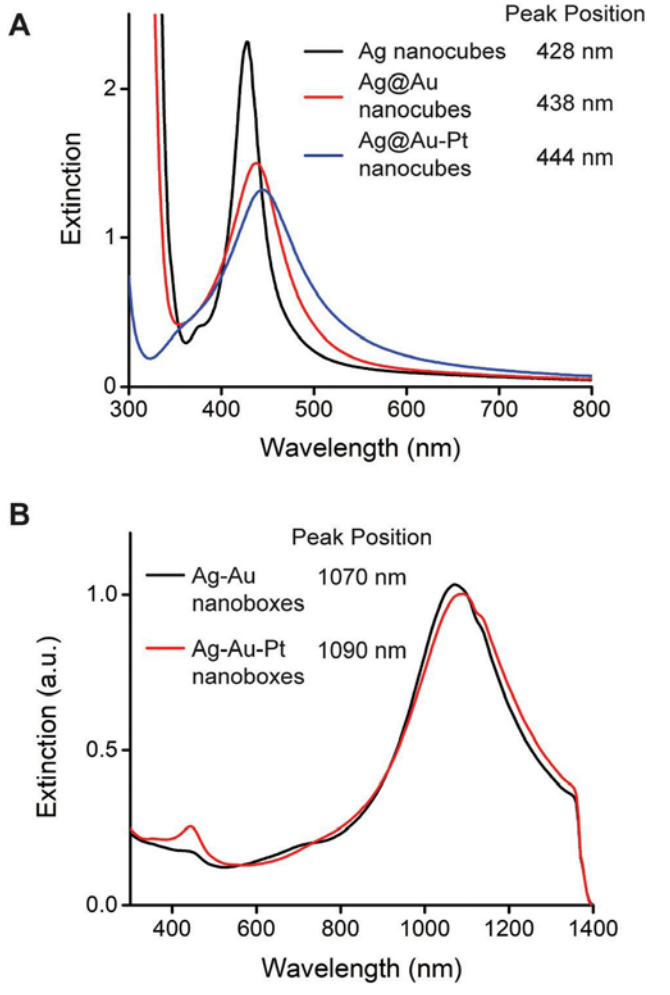


Fig. 7 (A) UV-vis spectra of the Ag nanocubes, Ag@Au nanocubes prepared with 0.8 mL of $HAuCl_4$, and Ag@Au–Pt trimetallic nanocubes prepared with 0.8 mL of $HAuCl_4$ and then 50 μL of $H_2PtCl_6$. (B) UV-vis-NIR spectra recorded from aqueous suspensions of the resultant Ag–Au and Ag–Au–Pt nanoboxes after etching of the Ag@Au and Ag@Au–Pt nanocubes shown in (A) with 3% aqueous $H_2O_2$.

## Conclusions

In summary, we demonstrated the transformation of Ag nanocubes into Ag@Au–Pt trimetallic nanocubes with Ag, Au, and Pt surface atoms enclosed on the {111}, {100}, and {110} facets of nanocubes, respectively. In a typical process, we started with Ag nanocubes to prepare for Ag@Au nanocubes with $Ag_2O$ patches on the {111} facets and Au on the {100} and {110} facets of nanocubes. Next, we dispersed as-obtained Ag@Au nanocubes to an aqueous solution containing $H_2Asc$ and PVP at pH = 3.2. Under an acidic condition, $H_2Asc$ could dissolve these $Ag_2O$ patches, making it possible for the underlying Ag atoms to be exposed on the {111} facets of the nanocubes. After the injection of different amounts of aqueous $H_2PtCl_6$ to the reaction solution, the added Pt precursor would be reduced by Ag *via* the galvanic replacement reaction and by $H_2Asc$ *via* chemical reduction to generate Pt atoms, followed by their preferential deposition on the {110} facets of nanocubes. As a result, the Ag@Au nanocubes were further converted into Ag@Au–Pt trimetallic nanocubes with well-defined facets enclosed by Ag, Au, and Pt atoms. We evaluated the SERS activities of the Ag@Au–Pt nanocubes by using 2,6-DMPI as a molecular probe to report the Pt atoms being deposited on the edges of the Ag@Au nanocubes where the SERS hot spots are located. We further demonstrated the use of these trimetallic nanoparticles with integrated plasmonic and catalytic properties for *in situ* monitoring the reduction of 4-NTP by $NaBH_4$ using SERS. After the removal of Ag in an aqueous

 

$H_2O_2$, we transformed the trimetallic nanocubes into Ag–Au–Pt nanoboxes with a wall thickness of ~2 nm and well-defined openings at the corners. These Ag–Au–Pt nanoboxes embrace strong plasmonic property with a major LSPR peak located in the near infrared region.

## Conflicts of interest

There are no conflicts to declare.

## Acknowledgements

We acknowledge the support from the National Science Foundation (CHE-1708300, CMMI-1634687), start-up funds from the Georgia Institute of Technology (GT), and a 3M non-tenured faculty award. We acknowledge the use of the characterization facility at the Institute of Electronics and Nanotechnology at GT. Z. Z. was also partially supported by the China Scholarship Council.

## Notes and references

1 H.-L. Jiang and Q. Xu, *J. Mater. Chem.*, 2011, **21**, 13705–13725.
2 H. Zhang, M. Okumura and N. Toshima, *J. Phys. Chem. C*, 2011, **115**, 14883–14891.
3 V. Mazumder, M. Chi, K. L. More and S. Sun, *J. Am. Chem. Soc.*, 2010, **132**, 7848–7849.
4 C. Wang, D. Van Der Vliet, K. L. More, N. J. Zaluzec, S. Peng, S. Sun, H. Daimon, G. Wang, J. Greeley, J. Pearson, A. P. Paulikas, G. Karapetrov, D. Strmcnik, N. M. Markovic and V. R. Stamenkovic, *Nano Lett.*, 2010, **11**, 919–926.
5 P.-P. Fang, S. Duan, X.-D. Lin, J. R. Anema, J.-F. Li, O. Buriez, Y. Ding, F.-R. Fan, D.-Y. Wu and B. Ren, *Chem. Sci.*, 2011, **2**, 531–539.
6 X. Sun, X. Yang, Y. Zhang, Y. Ding, D. Su and D. Qin, *Nanoscale*, 2017, **9**, 15107–15114.
7 J. Li, X. Sun and D. Qin, *ChemNanoMat*, 2016, **2**, 494–499.
8 J. W. Hong, S. W. Kang, B.-S. Choi, D. Kim, S. B. Lee and S. W. Han, *ACS Nano*, 2012, **6**, 2410–2419.
9 B. Lim, M. Jiang, P. H. Camargo, E. C. Cho, J. Tao, X. Lu, Y. Zhu and Y. Xia, *Science*, 2009, **324**, 1302–1305.
10 Z. Peng and H. Yang, *J. Am. Chem. Soc.*, 2009, **131**, 7542–7543.
11 M. Rycenga, C. M. Cobley, J. Zeng, W. Li, C. H. Moran, Q. Zhang, D. Qin and Y. Xia, *Chem. Rev.*, 2011, **111**, 3669–3712.
12 K. D. Gilroy, A. Ruditskiy, H.-C. Peng, D. Qin and Y. Xia, *Chem. Rev.*, 2016, **116**, 10414–10472.
13 J. Ahn, D. Wang, Y. Ding, J. Zhang and D. Qin, *ACS Nano*, 2018, **12**, 298–307.
14 Y. Wu, X. Sun, Y. Yang, J. Li, Y. Zhang and D. Qin, *Acc. Chem. Res.*, 2017, **50**, 1774–1784.
15 J. Li, J. Liu, Y. Yang and D. Qin, *J. Am. Chem. Soc.*, 2015, **137**, 7039–7042.
16 J. Li, Y. Wu, X. Sun, J. Liu, S. A. Winget and D. Qin, *ChemNanoMat*, 2016, **2**, 786–790.
17 J. Zhang, S. A. Winget, Y. Wu, D. Su, X. Sun, Z.-X. Xie and D. Qin, *ACS Nano*, 2016, **10**, 2607–2616.
18 Y. Wu, D. Su and D. Qin, *ChemNanoMat*, 2017, **3**, 245–251.
19 S. Xie, S.-I. Choi, X. Xia and Y. Xia, *Curr. Opin. Chem. Eng.*, 2013, **2**, 142–150.
20 B. Roldan Cuenya, *Acc. Chem. Res.*, 2013, **46**, 1682–1691.
21 S. Khanal, G. Casillas, J. J. Velazquez-Salazar, A. Ponce and M. Jose-Yacaman, *J. Phys. Chem. C*, 2012, **116**, 23596–23602.
22 L. Wang and Y. Yamauchi, *Chem. Mater.*, 2011, **23**, 2457–2465.
23 L. Wang and Y. Yamauchi, *J. Am. Chem. Soc.*, 2010, **132**, 13636–13638.
24 S. W. Kang, Y. W. Lee, Y. Park, B.-S. Choi, J. W. Hong, K.-H. Park and S. W. Han, *ACS Nano*, 2013, **7**, 7945–7955.
25 R. G. Weiner and S. E. Skrabalak, *Chem. Mater.*, 2016, **28**, 4139–4142.
26 E. González, J. Arbiol and V. F. Puntes, *Science*, 2011, **334**, 1377–1380.
27 Y. Yang, J. Liu, Z.-W. Fu and D. Qin, *J. Am. Chem. Soc.*, 2014, **136**, 8153–8156.
28 X. Sun, Y. Yang, Z. Zhang and D. Qin, *Chem. Mater.*, 2017, **29**, 4014–4021.
29 H. L. Johnston, F. Cuta and A. B. Garrett, *J. Am. Chem. Soc.*, 1933, **55**, 2311–2325.
30 X. Sun, J. Kim, K. D. Gilroy, J. Liu, T. A. F. König and D. Qin, *ACS Nano*, 2016, **10**, 8019–8025.
31 Q. Zhang, W. Li, L.-P. Wen, J. Chen and Y. Xia, *Chem. – Eur. J.*, 2010, **16**, 10234–10239.
32 Y. Zhang, J. Liu, J. Ahn, T.-H. Xiao, Z.-Y. Li and D. Qin, *ACS Nano*, 2017, **11**, 5080–5086.
33 K. Kim, K. L. Kim, J.-Y. Choi, H. B. Lee and K. S. Shin, *J. Phys. Chem. C*, 2010, **114**, 3448–3453.
34 S.-W. Joo, W.-J. Kim, W. S. Yun, S. Hwang and I. S. Choi, *Appl. Spectrosc.*, 2004, **58**, 218–223.
35 S. M. Ansar, F. S. Ameer, W. Hu, S. Zou, C. U. Pittman and D. Zhang, *Nano Lett.*, 2013, **13**, 1226–1229.